

Chapter 1

THE PHYSICS OF GLOBAL OPTIMIZATION OF ATOMIC CLUSTERS

Jonathan P. K. Doye

University Chemical Laboratory, Lensfield Road, Cambridge CB2 1EW, United Kingdom
 jon@clust.ch.cam.ac.uk

Abstract In this chapter the physical aspects of the global optimization of the geometry of atomic clusters are elucidated. In particular, I examine the structural principles that determine the nature of the lowest-energy structure, the physical reasons why some clusters are especially difficult to optimize and how the basin-hopping transformation of the potential energy surface enables these difficult clusters to be optimized.

Keywords: atomic clusters, basin-hopping, multiple funnels

1. INTRODUCTION

Global optimization (GO) is essentially a mathematical task. Namely, for the class of GO problems I will be particularly considering here, it is to find the absolute minimum (or maximum) of a cost function, $f(\mathbf{x})$, where \mathbf{x} belongs to a subset D of Euclidean n-space, \mathcal{R}^n , i.e.

$$\text{find } \mathbf{x}^* \text{ such that } f(\mathbf{x}^*) \leq f(\mathbf{x}) \quad \forall \mathbf{x} \in D \subset \mathcal{R}^n \quad (1.1)$$

Although the applications of global optimization span a wide range of fields—from the economics of business in the travelling salesman problem to biophysics in the lowest-energy structure of a protein—this does not take away from the essentially mathematical nature of the optimization problem.

So why do I wish to discuss the *physics* of global optimization. To begin with we should realize that even for GO problems that do not correspond to a physical system, physical properties can be associated with the system by thinking of the cost function as a potential energy function, $E(\mathbf{x})$. This allows the thermodynamics of the system to be defined. When the system is at equilibrium at a temperature T each point \mathbf{x} in configuration space will be sampled

with a probability proportional to its Boltzmann weight, $\exp(-E(\mathbf{x})/kT)$, where k is the Boltzmann constant. Furthermore, for systems with continuous coordinates the forces, $F(\mathbf{x})$, associated with each coordinate can be obtained from the gradient of the cost function, i.e. $F(\mathbf{x}) = -\nabla E(\mathbf{x})$. Once masses are associated with each coordinate, the dynamics are then defined through Newton's equations of motion. If one wishes the system's dynamics can then be simulated by integrating these equations of motion, as in the molecular dynamics method [1]. Even when the coordinates can only take discrete values, Monte Carlo (MC) simulations can still provide a pseudo-dynamics with the number of steps taking the role of time.

Of course, this connection to physics is most transparent, and most natural, when the system being optimized is a physical system, which has a real (and potentially observable) thermodynamics and dynamics. Furthermore, in those cases where the cost function does truly correspond to the potential energy of the system, there is another physical dimension to the problem—how is the structure of the global minimum determined by the physical interactions between the atoms and molecules that make up $E(\mathbf{x})$.

Given that we have established that physical properties can be associated with any system being optimized, what relevance does this physics have to the task of global optimization. Firstly, many GO algorithm have drawn their inspiration from physics. Most famously, simulated annealing is analogous to the slow cooling of a melt to allow the formation of a near perfect crystal, the idea being that if equilibrium is maintained in the simulation as the system is cooled, then at zero temperature it must end up in the global minimum [2]. And there are many other physically-motivated GO approaches: The extension of statistical thermodynamics to systems with non-extensive thermodynamics through the use of Tsallis statistics [3, 4] has led to a generalized simulated annealing [5, 6] which is no longer tied to the Boltzmann distribution and is often more efficient than standard simulated annealing. Genetic algorithms imitate the biophysical evolution of the genome [7]. And I could go on.

However, this is not the role of physics in global optimization that is my focus here. Rather, I wish to show how the ease or difficulty of global optimization is often intimately linked to the physics of the system. The insights obtained from understanding the physical basis for the success or failure of an algorithm not only provide an understanding of the limitations of the method and a basis for assessing the likelihood of success in future applications, but also aid the development of new algorithms by identifying the main physical challenges that need to be overcome to enable greater efficiency and suggesting the type of physical behaviour that would need to be incorporated into an improved algorithm.

I will attempt to achieve this aim by concentrating on one class of problems, namely the global minimization of the potential energy of an atomic clus-

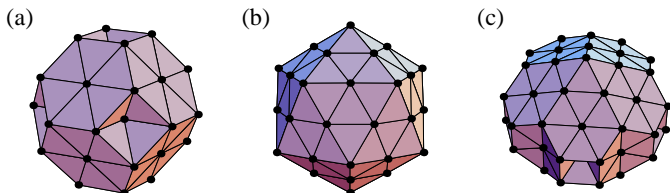


Figure 1.1 Three examples of the structures clusters can adopt: (a) a 38-atom truncated octahedron, (b) a 55-atom Mackay icosahedron, and (c) a 75-atom Marks' decahedron. These clusters have the optimal shape for the three main types of regular packing seen in clusters: close-packed, icosahedral and decahedral, respectively. The Mackay icosahedron is a common structure and is observed for rare gas [10] and many metal [11] clusters. The truncated octahedron has been recently observed for nickel [12] and gold [13] clusters, and the Marks decahedron for gold clusters [14].

ter. Furthermore, I will mainly concentrate on model systems where the cost function is relatively computationally cheap to evaluate, enabling the physical properties of these systems to be comprehensively examined and understood. As outlined by Hartke elsewhere in this book [8], this class of problems is of great general interest to the chemical physics community, because the identification of a cluster's structure is often a prerequisite for understanding its other physical and chemical properties.

In this chapter I start at the 'end', first showing the structures of the global minima for a number of cluster systems in order that the reader can understand some of the physical principles that determine the structure and how these relate to the interatomic interactions. Furthermore, the structure provides a basis for understanding a cluster's thermodynamic and dynamic properties, especially when, as in some of our examples, the competition between different structural types plays an important role.

I then consider some of the GO algorithms that are most successful for these systems focussing on those that use the basin-hopping transformation of $E(\mathbf{x})$ [9] and on how the performance of these algorithms depend on the system and the cluster size. I then look at the physical properties of some of the clusters, relating these back to the ease or difficulty of global optimization. I firstly examine the topography of the multi-dimensional surface defined by $E(\mathbf{x})$ (the so-called potential energy surface (PES) or energy landscape), then the thermodynamics and dynamics. Finally, I show why basin-hopping is able to locate the global minimum in those clusters where the PES has a multiple-funnel topography, and make some suggestions as to how further gains in efficiency might be secured.

2. CLUSTER STRUCTURE

In this section I will mainly concentrate on the structures of model clusters, where the interactions have simple idealized forms that are isotropic, thus

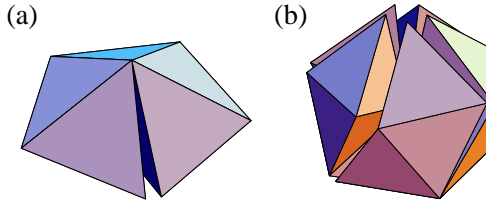


Figure 1.2 Examples of the strain involved in packing tetrahedra. (a) Five regular tetrahedra around a common edge produce a gap of 7.36°. (b) Twenty regular tetrahedra about a common vertex produce gaps equivalent to 1.54 steradians.

favouring compact geometries. The models have been chosen so that they span a wide range of structural behaviour that is likely to be relevant to rare gas, metal and molecular clusters bound by dispersion forces, but not to clusters with directional covalent bonding or molecular clusters with directional intermolecular forces, as with the hydrogen bonding in water clusters.

Most of the clusters we consider have only pair interactions, i.e.

$$E(\mathbf{x}) = \sum_{i < j} V(r_{ij}), \quad (1.2)$$

where V is the pair potential and r_{ij} is the distance between atoms i and j . In this case we can partition the energy into three terms [15]:

$$E = -n_{\text{nn}}\epsilon + E_{\text{strain}} + E_{\text{nnn}} \quad (1.3)$$

where ϵ is the pair well depth, n_{nn} is the number of nearest neighbours (two atoms are defined as nearest neighbours if $r_{ij} < r_0$),

$$E_{\text{strain}} = \sum_{i < j, r_{ij} < r_0} (V(r_{ij}) + \epsilon) \text{ and } E_{\text{nnn}} = \sum_{i < j, r_{ij} \geq r_0} V(r_{ij}). \quad (1.4)$$

The first term in Equation 1.3 is the ideal pair energy if all n_{nn} nearest-neighbour pairs lie exactly at the equilibrium pair distance, the strain energy is the energetic penalty for the deviation of nearest-neighbour distances from the equilibrium pair distance and E_{nnn} is the contribution to the energy from non-nearest neighbours.

E_{nnn} is usually smaller than the other two terms and is relatively independent of the detailed structure. Therefore, the global minimum usually represents the best balance between maximizing n_{nn} and minimizing E_{strain} . For an atom in the interior of a cluster this is usually achieved through the atom having a coordination number of twelve. This can be achieved as in close-packing, but another possibility is an icosahedral coordination shell. n_{nn} is further maximized through the cluster having a compact spherical shape, and through the surface mainly consisting of faces with a high co-ordination number. For

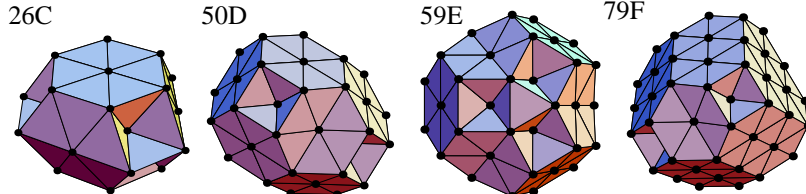


Figure 1.3 Four examples of stable close-packed structures for $N < 80$. The sizes are as labelled. The 59-atoms structure has T_d point group symmetry, and the rest D_{3h} .

example, an atom on a face-centred-cubic (fcc) $\{111\}$ face has nine nearest neighbours, whereas an atom on a $\{100\}$ face has eight nearest neighbours.

The three main types of cluster structure found for systems with isotropic interactions, namely icosahedral, decahedral and close-packed structures, are depicted in Figure 1.1. These examples have the optimal shape for each structural type, and all have been identified experimentally.

One of the unusual properties of clusters is that they can exhibit non-crystallographic symmetries, because there is no requirement for translational periodicity. Decahedral clusters have a single five-fold axis and are based on a pentagonal bipyramid that can be thought of as five strained fcc tetrahedra sharing a common edge. The symmetry axis corresponds to this common edge. The Marks decahedron [16], which represents the optimal shape for this structural type, can be formed from a pentagonal bipyramid by exposing $\{100\}$ faces at the equatorial edges then introducing reentrant $\{111\}$ faces. Mackay icosahedra [17] have six five-fold axes of symmetry and can be thought of as twenty strained fcc tetrahedra sharing a common edge. The fcc cluster represented in Figure 1.1a is simply a fragment of the bulk fcc lattice.

Icosahedral structures generally have the largest n_{nn} because of their spherical shape and $\{111\}$ faces, and close-packed clusters the smallest n_{nn} because of their higher proportion of $\{100\}$ faces. By contrast, close-packed clusters can be unstrained, whereas, as Figure 1.2 illustrates, decahedra and icosahedra are increasingly strained. The strain energy is proportional to the volume of the cluster, but differences in n_{nn} are due to surface effects. Therefore, icosahedra are likely to be found at small sizes, but at sufficiently large size, the cluster must take on the bulk structure. At intermediate sizes decahedra can be most stable. The sizes at which the crossovers between structural types occurs is dependent on system.

The structures illustrated in Figure 1.1 involve exactly the right number of atoms to form a cluster of the optimal shape. For example, complete Mackay icosahedra can be formed at $N = 13, 55, 147, 309, \dots$. At intermediate sizes clusters have an incomplete surface layer. Marks decahedra with square $\{100\}$ faces occur at $N = 75, 192, 389, \dots$. Other complete Marks decahedra that are less spherical can be found in between these sizes, e.g. at $N=101$ and

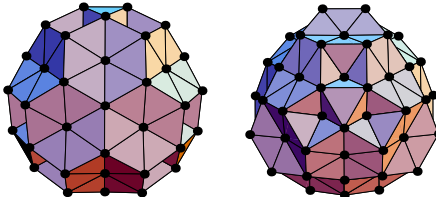


Figure 1.4 Front and back views of the 98-atom Leary tetrahedron.

146. Fcc truncated octahedra with regular hexagonal $\{111\}$ faces can be found at $N = 38, 201, 586 \dots$, and other less spherical truncated octahedra can be found, for example, at $N=79, 116, 140$ [18]. Furthermore, because the energy of a twin plane is often small, close-packed structures with other forms can also be particularly stable. Four examples are given in Figure 1.3 for $N < 100$. The 26-atom structure has a hexagonal close-packed (hcp) structure; the 50-atom structure consists of two fragments of the 38-atom structure joined at a twin plane; the 59-atom structure consists of a 31-atom fcc truncated tetrahedron with each face covered by a 7-atom hexagonal overlayer that occupies the hcp surface sites; and the 79-atom structure, which is similar to the 50-atom structure, is formed by the introduction of a twin plane into the 79-atom truncated octahedron [19].

Recently, a new structural type called a Leary tetrahedron [20] has been discovered. An example with 98-atoms is illustrated in Figure 1.4. At the centre of this structure is an fcc tetrahedron. To each of the faces of this tetrahedron, further fcc tetrahedra (minus an apical atom) are added, to form a stellated tetrahedron. Finally, the edges of the original tetrahedron are covered by 7-atom hexagonal overlayers. The coordination along the edges of the central tetrahedron is the same as along the symmetry axis of the decahedron and so the strain energy of this structure is intermediate between icosahedra and decahedra. It is not yet clear how general this class of structures is. The 98-atom example is the global minimum for a model potential [20] and mass spectroscopic studies of clusters of C_{60} molecules suggest that $(C_{60})_{98}$ has this structure [21]. However, it may be that the stability of this structural class is restricted to $N=98$, because this size results in a particularly spherical shape, and that equivalent structures at larger sizes (e.g. $N=159, 195$) are never competitive.

2.1 LENNARD-JONES CLUSTERS

In this section I focus on clusters bound by the Lennard-Jones (LJ) potential [22]:

$$E = 4\epsilon \sum_{i < j} \left[\left(\frac{\sigma}{r_{ij}} \right)^{12} - \left(\frac{\sigma}{r_{ij}} \right)^6 \right], \quad (1.5)$$

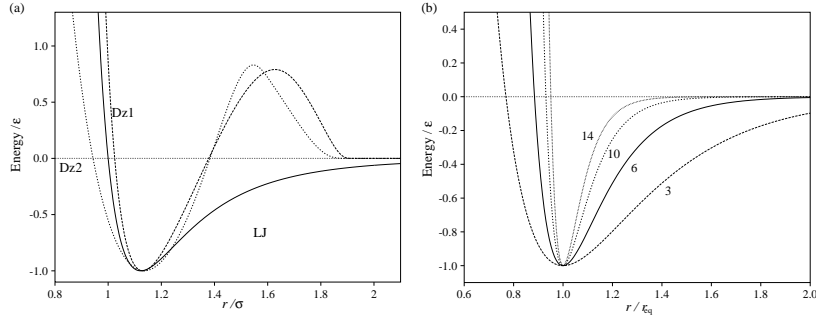


Figure 1.5 (a) A comparison of the Lennard-Jones (LJ) potential with the Dzugutov potential (Dz1) and a modified version of it (Dz2). (b) The Morse potential for several values of the range parameter, ρ .

where ϵ is the pair well depth and $2^{1/6}\sigma$ is the equilibrium pair separation. The potential is illustrated in Figure 1.5a, and provides a reasonable description of the interatomic interactions of rare gases, such as argon. This system has become probably the most common test system for GO algorithms for configurational problems. The number of papers with applications to this system is now very large, but unfortunately many are distinctly unimpressive, only reporting results for small sizes or failing for relatively simple cases. I do not attempt to review this literature, but instead refer the interested reader elsewhere [23].

At small sizes the LJ potential is able to accommodate the strain associated with icosahedral packing relatively easily [24]. Indeed, only for $N > 1600$ are the majority of global minimum expected to be decahedral and the crossover to fcc clusters has been estimated to occur at $N \approx 10^5$ [19]. This preference for icosahedral packing is also evident from Figure 1.6 where I compare the energies of icosahedral, decahedral and close-packed clusters. Sizes where complete Mackay icosahedra are possible ($N=13, 55$) stand out as particularly stable. The icosahedra are least stable when the overlayer is roughly half-filled. Therefore, when especially stable non-icosahedral clusters coincide with these sizes there is a possibility that the global minimum will be non-icosahedral. There are eight such cases for $N \leq 147$. At $N=38$ the global minimum is the fcc truncated octahedron [15, 25, 26] (Figure 1.1); at $N=75-77$ [15] and 102–104 [18] the global minima are Marks decahedra; and at $N=98$ the global minimum is a Leary tetrahedron [20]. At these sizes the lines for the decahedral or close-packed structures in Figure 1.6 dip just below the line for the icosahedra. For $148 \leq N \leq 309$ there are a further eight non-icosahedral global minima [8, 27], all of which are decahedral and which divide into two sets based on the complete Marks decahedra possible at $N=192$ and 238.

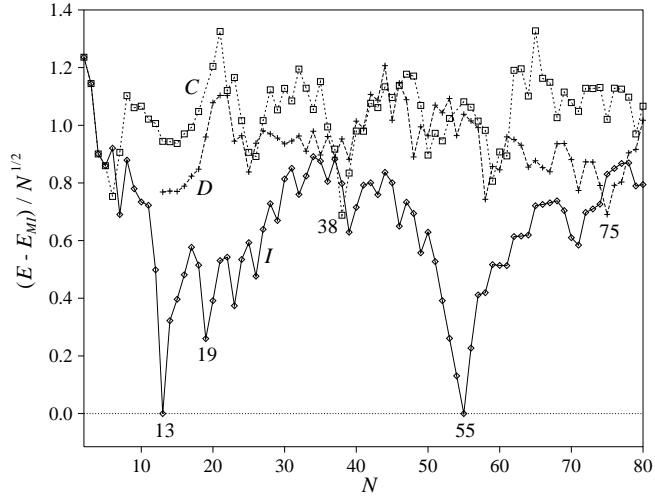


Figure 1.6 Comparison of the energies of icosahedral (I), decahedral (D) and close-packed (C) LJ_N clusters. The energy zero is E_{MI} , a function fitted to the energies of the first four Mackay icosahedra at $N=13, 55, 147$ and 309 :

2.2 MORSE CLUSTERS

In this section I focus on clusters bound by the the Morse potential [28]:

$$V_M = \epsilon \sum_{i < j} e^{\rho(1-r_{ij}/r_{\text{eq}})} (e^{\rho(1-r_{ij}/r_{\text{eq}})} - 2), \quad (1.6)$$

where ϵ is the pair well depth and r_{eq} is the equilibrium pair separation. In reduced units there is a single adjustable parameter, ρ , which determines the range of the interparticle forces. Figure 1.5b shows that decreasing ρ increases the range of the attractive part of the potential and softens the repulsive wall, thus widening the potential well. Values of ρ appropriate to a range of materials have been catalogued elsewhere [29]. The LJ potential has the same curvature at the bottom of the well as the Morse potential when $\rho = 6$. Girifalco has obtained an intermolecular potential for C_{60} molecules [30] that is isotropic and short-ranged relative to the equilibrium pair separation with an effective value of $\rho = 13.62$ [31]. The alkali metals have longer-ranged interactions, for example $\rho=3.15$ has been suggested for sodium [32].

The global minima for this system have been found as a function of ρ for all sizes up to $N=80$ [15, 33].¹ Equation (1.3) enables us to understand the effect of ρ on cluster structure. As ρ increases and the potential well narrows, the energetic penalty for distances deviating from the equilibrium pair separation increases. Thus, E_{strain} increases for strained structures, and so icosahedral and decahedral structures become disfavoured as ρ increases. This is illustrated in Figure 1.7, which shows how the structure of the global minimum depends on

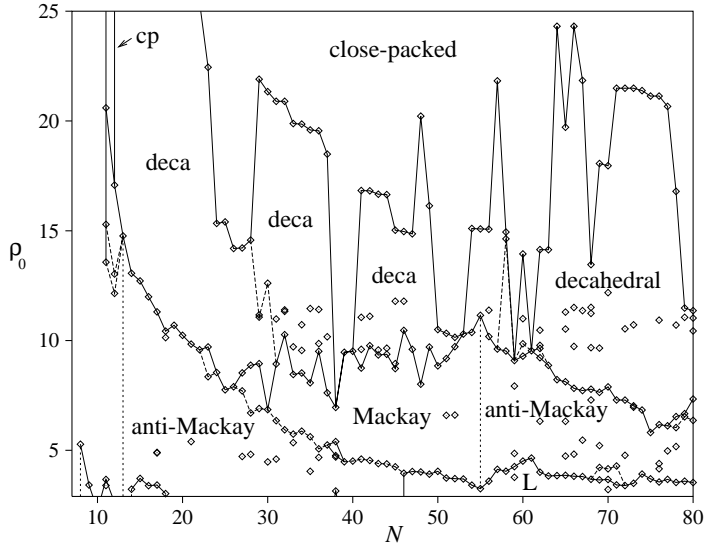


Figure 1.7 Zero temperature ‘phase diagram’ showing the variation of the lowest-energy structure with N and ρ . The data points are the values of ρ at which the global minimum changes. The lines joining the data points divide the phase diagram into regions where the global minima have similar structures. The solid lines denote the boundaries between the four main structural types—icosahedral, decahedral, close-packed and those associated with low ρ (L)—and the dashed lines are internal boundaries within a structural type, e.g. between icosahedra with Mackay and anti-Mackay overlayers, or between decahedra with different length decahedral axes.

N and ρ . The global minimum generally change from icosahedral to decahedral to close-packed as ρ is increased. It can be seen that the value of ρ appropriate for the LJ potential lies roughly in the middle of the icosahedral region of Figure 1.7.

Alternatively, the effect of ρ can be thought of in terms of how it affects the crossover sizes at which a particular structural type becomes dominant. As ρ increases, the less strained structures become dominant at smaller sizes. These effects can also be found in real materials. For example, sodium clusters have been shown to exhibit icosahedral structures up to at least 22 000 atoms [34], whereas the thermodynamically stable structure of clusters of C_{60} molecules have recently been shown to be non-icosahedral for $N > 30$ [21].

As well as these trends, Figure 1.7, of course, also reflects the specifics of the structures that are possible at each size, so the boundaries between structural types are not smooth lines but show a lot of detailed structure. For example, the range of ρ values for which icosahedral structures are most stable is a local maximum at $N=55$ because of the complete Mackay icosahedra possible at this size. At sizes where close-packed structures have a greater or equal number of

nearest numbers to the best decahedral structure, the global minimum changes directly from icosahedral to close-packed.

A new class of structures appears in the bottom right-hand corner of Figure 1.7. They are polytetrahedral clusters with disclination lines running through them. A polytetrahedral structure can be decomposed into tetrahedra without any interstices. The 13-atom icosahedron is an example, and one of the possible ways of adding atoms to the surface of the icosahedron—the so-called anti-Mackay overlayer—continues the polytetrahedral packing. This overlayer does not lead to the next Mackay icosahedron but instead to the 45-atom rhombic tricontahedron (Figure 1.8a), which can be thought of as an icosahedra of interpenetrating icosahedra. If one imagines adding regular tetrahedra to the form in Figure 1.2b one soon realizes that the 45-atom structure must be extremely strained, and for this reason it is the global minimum only at low ρ , where this strain can be accommodated. For $N > 45$ similar polytetrahedral clusters can be formed but based not on the 13-atom icosahedron but on polyhedra with a higher coordination number. The two examples in Figure 1.8a have a 14- and 16-coordinate central atom. These structures can be described in terms of disclination lines, where the lines pass along those nearest-neighbour contacts that are the common edge for six tetrahedra [35]. These types of structures might be thought to be fairly esoteric, but they form the basis for the crystalline Frank-Kasper phases [36, 37] where atoms of different size create a preference for coordination numbers higher than 12, and so they might be good candidate structures for certain mixed metal clusters. Furthermore, recent experimental diffraction data for small cobalt clusters can best be modelled by a disclinated polytetrahedral structure that is a fragment of a Frank-Kasper phase [38]. However, at the size corresponding to this experiment ($N \approx 150$) the long-ranged Morse clusters have disordered polytetrahedral global minima.

2.3 DZUGUTOV CLUSTERS

In contrast to the potentials that we have so far examined, the Dzugutov potential [39] has a maximum that penalizes distances near to $\sqrt{2}$ times the equilibrium pair distance (Figure 1.5a), the distance across the diagonal of the octahedra in close-packed structures. This maximum loosely resembles the first of the Friedel oscillations often found in effective metal potentials. The potential was originally designed to suppress crystallization in bulk simulations so that the properties of supercooled liquids and glasses could more easily be studied in a one-component system [39, 40]. However, under certain conditions it was found that a dodecagonal quasicrystal could be formed on freezing [41].

For clusters the potential will penalize close-packed, decahedral and Mackay icosahedral structures (the latter two because octahedra are found within the fcc tetrahedral units from which the structures are made) and will favour polyte-

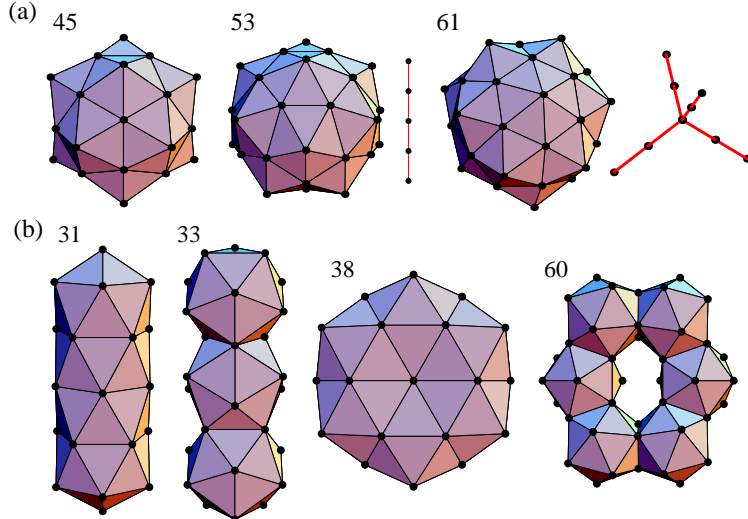


Figure 1.8 Polytetrahedral structures that are the global minima for the (a) long-ranged Morse potential and (b) Dzugutov potential. Sizes as labelled. The point group symmetries of the structures in (a) are I_h , D_{6d} and T_d and in (b) are D_{5h} , D_{3d} and D_{6h} and C_s . The disclination networks associated with the 53- and 61-atom structures are illustrated next to the clusters.

trahedral clusters. Therefore, one might think that this potential would provide a good model for small cobalt clusters. However, as can be seen from Figure 1.5a the potential is narrower than the LJ potential, and matching the second derivative at the equilibrium pair separation to that of the Morse potential gives an effective value of ρ of 7.52. Therefore, the potential cannot accommodate the strain in compact polytetrahedral clusters. Instead, the global minima are non-compact polytetrahedral structures, such as the needles, disc and torus illustrated in Figure 1.8b. These structures are made up of face-sharing or interpenetrating 13-atom icosahedral units. In terms of Equation (1.3) they represent the best balance between maximizing n_{nn} whilst minimizing both E_{strain} and E_{nnn} , where the latter now corresponds to the total energetic penalty for distances close to $\sqrt{2} r_{\text{eq}}$.

In order to generate a model that exhibits ordered compact polytetrahedral clusters a modified Dzugutov potential was constructed with an effective value of ρ of 5.16, allowing it to accommodate more strain (Figure 1.5a). Preliminary results indicate that the global minima do have the desired structural type, and so this system should be useful in generating realistic candidate structures to compare with the cobalt experiments.

2.4 COMPARISON WITH EXPERIMENT

One of the remarkable features of these simple model potentials is that the structures they exhibit do provide good candidates for the structures of real clusters. Indeed, frequently the structures first identified for these model systems are subsequently identified in experiments. For example, the especial stability of the structures of the fcc Ni_{38} [12] and Au_{38} [13], the decahedral Au_{75} [14] and the tetrahedral $(\text{C}_{60})_{98}$ [21] were first identified through calculations on LJ and Morse clusters [15, 20].

Furthermore, as experiments can rarely detect the structure directly, but often have to rely on comparison with properties calculated using candidate structures, it is extremely useful to have databases of plausible structures available. This is the philosophy behind internet repositories such as the Cambridge Cluster Database (<http://brian.ch.cam.ac.uk/CCD.html>), which contains the global minima for all the potentials described here, and the Birmingham Cluster website (<http://www.tc.bham.ac.uk/bcweb/>).

In comparisons between experiment and theory the role of temperature and kinetics should be remembered. The global minimum is only rigorously the equilibrium structure at zero temperature. At higher temperatures other structures may become more stable due to entropic effects [42, 43] as we will see in Section 4.1. Furthermore, it is not always clear whether equilibrium has been achieved under the experimental conditions, especially for clusters formed at low temperature [21, 44].

3. GLOBAL OPTIMIZATION APPROACHES

The type of GO algorithms in which I am interested are those that find global minima, not those that are also able to *prove* that the best structure found is in fact truly global.² Unsurprisingly, the latter is a much more demanding task. For example, for LJ clusters good putative global minima have been found up to $N=309$, but only up to $N=7$ have these structures been proven to be global [45]. Of course, the problem with settling for obtaining putative global minima is that it is difficult to know when to give up looking for a lower-energy solution. For example, to my surprise, at least, a new putative global minimum was recently found for LJ_{98} [20], even though powerful GO algorithms had previously been applied to this cluster [9, 46, 47, 48]. The failure of these previous attempts to locate the global minimum was not because the algorithms are unable to locate the Leary tetrahedron, but simply because the computations had been terminated too soon.

I also wish to concentrate on GO algorithms that are unbiased, i.e. those that do not artificially bias the system towards those structures that physical insight would suggest are low in energy, for example, by seeding the algorithm with fragments of a certain structural type [48] or by searching on a lattice for a

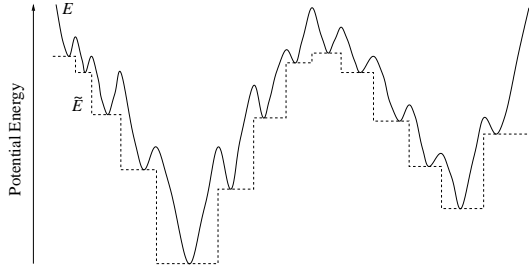


Figure 1.9 A schematic diagram illustrating the effects of the basin-hopping potential energy transformation for a one-dimensional example. The solid line is the potential energy of the original surface and the dashed line is the transformed energy, \tilde{E} .

specified structural type [24]. Of course, such biased algorithms are usually more efficient. For example, most of the LJ global minima were first found using such methods [24, 27]. However, they cannot cope with ‘surprising’ structures that fall outside the expected categories, and lack transferability to other systems, because they have sacrificed generality for greater efficiency in the specific problem instances. Furthermore, they require a sufficient prior understanding of the structure. This may be possible for the model potentials we consider here, but it is a much more difficult task with the complex interactions that are often necessary to realistically describe a system.

Virtually all the global optimization algorithms that are most successful at locating the global minima of clusters have a common feature. Namely, they make extensive use of local minimization. All GO algorithms require elements of both local and global search. The algorithm has both to be able to explore all regions of configuration space (overcoming any energy barriers that might hinder this) whilst also sufficiently sampling the low-energy configurations within each region. Performing local minimizations from configurations generated by a global search is one way of combining these two elements.

Simulated annealing provides a perhaps more traditional way of achieving this goal. In simulated annealing, by varying a parameter, the temperature, the nature of the search is changed from global (at high temperature) to local (as $T \rightarrow 0$). However, this approach has a number of weaknesses. There is effectively only one local minimization, so if the configuration does not become confined to the basin of attraction of the global minimum as the temperature is reduced the algorithm will fail, even if the system had passed through that basin of attraction at higher temperature. This condition for success is unnecessarily restrictive and leads to inefficiency.

There is a further element to the most successful algorithms, namely that the energies of the local minima, not of the configurations prior to minimization, are the basis for comparing and selecting structures. This approach was first used in 1987 by Li and Scheraga in the application of their ‘Monte Carlo

plus minimization' to polypeptides [49]. However, despite this approach being independently adopted a number of times subsequently [50, 51], it was only in 1997 that it was realized that in this approach one is effectively searching a transformed PES, $\tilde{E}(\mathbf{x})$, where the energy associated with each point in configuration space is that of the minimum obtained by a local minimization from that point [9], i.e.

$$\tilde{E}(\mathbf{x}) = \min\{E(\mathbf{x})\}, \quad (1.7)$$

where 'min' signifies that an energy minimization is carried out starting from \mathbf{x} . Unlike many PES transformations proposed in the name of global optimization, this 'basin-hopping' transformation is guaranteed to preserve the identity of the global minimum. The transformation maps the PES onto a set of interpenetrating staircases with plateaus corresponding to the basins of attraction of each minimum (i.e. the set of configurations which lead to a given minimum after optimization). A schematic view of the staircase topography that results from this transformation is given in Figure 1.9.

There are a number of advantages of using the basin-hopping transformation. Firstly, the transformation removes vibrational motion (the Hessian has no positive eigenvalues). If simulated, unlike on the untransformed PES, the system will no longer waste much of its time oscillating back and forth within a basin of attraction, waiting for a transition to another minimum. Secondly, transitions out of a basin can occur anywhere along the boundary of the basin, and not just along the transition state valley. Thirdly, downhill transitions are now barrierless. However, as Figure 1.9 illustrates, significant barriers between low-energy minima can remain if they are separated by high-energy intervening minima.

Consequently, on $\tilde{E}(\mathbf{x})$ the system can hop directly between basins; hence the name of this transformation. Furthermore, much larger MC steps can be taken on $\tilde{E}(\mathbf{x})$; such steps would virtually always be rejected on the original PES because atoms would become too close and an extremely high energy would result. After the transformation atoms can even pass through each other.

The method of searching $\tilde{E}(\mathbf{x})$ is of secondary importance compared to the use of the transformation itself. Indeed, the performance is fairly similar for the two main methods used, genetic algorithms and the constant temperature MC used in basin-hopping. Here, we mainly concentrate on the basin-hopping approach and refer readers to Hartke's chapter for more detail on the genetic algorithm methodology [8].

In the basin-hopping or Monte Carlo plus minimization method, standard Metropolis MC is used, i.e. moves are generated by randomly perturbing the coordinates, and are always accepted if \tilde{E} decreases and are accepted with a probability $\exp(-\Delta\tilde{E}/kT)$ if \tilde{E} increases. Using constant temperature is sufficient, since there is no great advantage to using an annealing schedule because the aim is not to trap the system in the global minimum, but just

to visit it at some point in the simulation. One of the advantages of this method is its simplicity—there are few parameters to adjust. It is usually satisfactory to dynamically adjust the step size to produce a 50% acceptance ratio. An appropriate temperature also needs to be chosen, but fortunately the temperature window for which the method is effective is usually large, and can be quickly found after some experimentation. Furthermore, there is a well-defined thermodynamics associated with the method [52] that makes understanding the physics behind the approach easier, as we shall see in Section 4.3.

Typically, a series of basin-hopping runs of a specified length will be performed starting from a random geometry. This is advantageous over a single longer run because it can provide a loose gauge of success. If all the runs return the same lowest-energy structure one would imagine that the true global minimum had been found. It can also often prove useful to perform runs starting from the best structures at sizes one above and below, with the lowest-energy atom removed or an atom added, respectively.

The local minimization method that we have found to be most efficient for clusters is a limited memory BFGS algorithm [53]. The basin-hopping approach is also found to be more efficient when the configuration is reset to the configuration of the local minimum after each accepted step [54]; this avoids problems with evaporation of atoms from the cluster since the basin-hopping transformation also reduces the barriers to dissociation. In addition to the usual steps, it is advantageous to have occasional angular steps for low-energy surface atoms. These have a similar aim to the directed mutations introduced by Hartke into his genetic algorithm [47]; they both enable the best arrangement of the surface atoms to be found more rapidly. For biopolymers other system-specific step types have been introduced to increase efficiency [55].

One of the main differences between the basin-hopping and genetic algorithms is that only local moves are used in basin-hopping, whereas genetic algorithms employ co-operative crossover moves in which a new structure is formed from fragments of two ‘parent’ clusters. However, recently non-local moves have been introduced into a variant of basin-hopping by rotating or reflecting a fragment of the structure [56].

Two examples of the performance of basin-hopping algorithms for LJ clusters as a function of size are given in Figure 1.10 and 1.11. The basin-hopping transformation must lead to a considerable speed-up (in terms of steps) if the method is to be cost-effective, because the transformation is computationally expensive and requires many evaluations of the energy and the forces at each step. Clearly, it would not be feasible to use the many millions of steps and cycles that are typically used in MD and MC simulations on the original PES. However, the results in Figure 1.10 show that the number of steps required to find the global minimum is remarkably few, only of the order of hundreds or

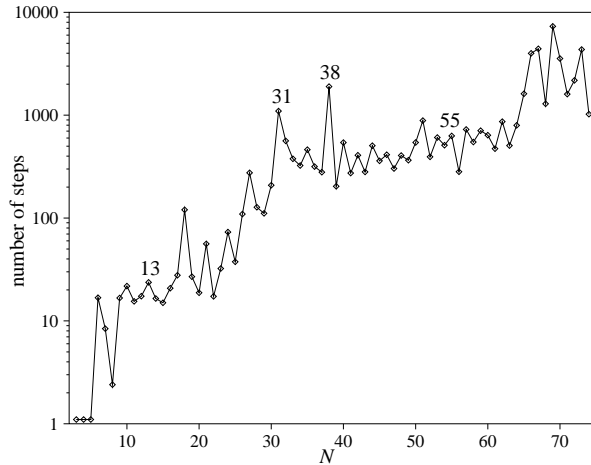


Figure 1.10 Mean number of steps to reach the LJ_N global minimum from a random starting point with the basin-hopping approach up to $N=74$. The average is over a hundred runs at $T = 0.8\epsilon k^{-1}$. Reproduced from Ref. [57].

thousands of steps. This is even more remarkable when the number of minima on the PES is considered. In line with theoretical expectations [58] the number of minima for small LJ clusters increases exponentially with size [59]. Extrapolating this trend provides, for example, an estimate of 10^{21} minima for LJ_{55} . Therefore, a Levinthal-type paradox [60]³ can be formulated for locating the global minimum of a cluster: the number of minima of an atomic cluster quickly becomes so large that beyond a fairly small size, if these minima were *randomly* searched, even at an extraordinarily fast rate, it would take an unfeasibly long time to locate the global minimum—so how is it possible to find the global minimum? Yet the basin-hopping algorithm using optimal parameters finds the LJ_{55} global minimum from a random starting configuration on average within 150 steps [57]. The fallacy in Levinthal’s paradox has long been known to be the assumption of random searching [61, 62, 63, 64] however it does emphasize the extremely non-random nature of basin-hopping for LJ_{55} —the runs are extremely biased towards the global minimum.

Figure 1.10 shows some interesting variations in the ease of global optimization with cluster size. The 38-atom global minimum particularly stands out as being difficult to locate, suggesting that competition between different structural types makes global optimization more difficult. Indeed for LJ_{75} , the next largest cluster with a non-icosahedral global minimum, the number of steps required is so large that it was not possible to obtain good statistics to be included in Figure 1.10. Subsequent calculations on a super-computer by Leary suggest that the mean first passage time is of the order of 10^7 steps [65]. The other six non-icosahedral global minima for $N < 150$ are of roughly similar

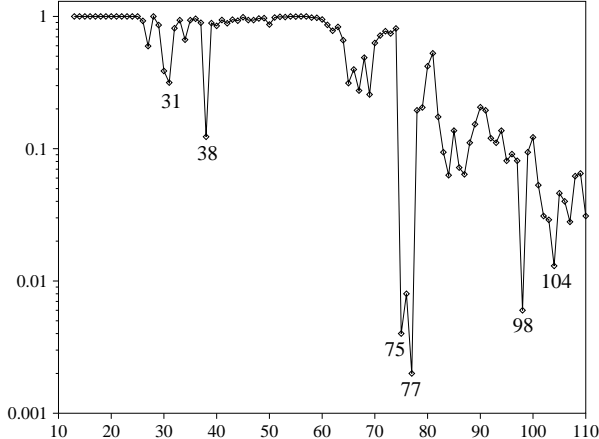


Figure 1.11 Observed probability of hitting the global minimum in a monotonic sequence basin-hopping run starting from a random starting point, averaged over 1000 runs. Reproduced from Ref. [65].

difficulty to locate. It is also noteworthy that the global minimum for LJ₃₁ is relatively difficult to find. In this case, there is some structural competition between the two types of icosahedral overlayer—it is the first size at which the overlayer that leads to the next Mackay icosahedron is lowest in energy.

An alternative perspective on these effects can be obtained from Figure 1.11, which shows the probability that a ‘monotonic sequence’ basin-hopping run ends at the global minimum. In this variation of the basin-hopping algorithm [65] only downhill steps are accepted (i.e. $T=0$) and the run is stopped after there is no further improvement for a certain number of steps. For those sizes with non-icosahedral global minima there is a much smaller probability of the run ending in the global minimum, and so again global optimization is more difficult. In these cases the majority of runs end at low-energy icosahedral structures. Those examples at larger sizes are again more than an order of magnitude more difficult than LJ₃₈, but interestingly the Marks decahedra at $N=102-104$ are somewhat more easy to locate than those at $N=75-77$.

These results enable us to comment on the use of LJ clusters as a test system for GO methods. They show that the icosahedral global minima are relatively easy to locate, and in these cases optimization only starts to become more difficult as N approaches 100 (Figure 1.11). As for the non-icosahedral global minima, the number of unbiased GO methods that have found the LJ₃₈ global minimum is now quite large [9, 26, 46, 47, 56, 65, 66, 67, 68, 69, 70, 71, 72] but those that can find the LJ₇₅ global minimum is still small [9, 47, 56, 65, 71]. Therefore, a good test for a GO method is to attempt to find all the global minima up to $N=110$. Any GO method ‘worth its salt’ should be able find all the icosahedral global minima and the truncated octahedron at $N=38$. Success

for the other non-icosahedral global minima would indicate that the method has particular promise. However, far too many GO algorithms have only been tested on sizes where global optimization is relatively trivial.

The weakness of LJ clusters as a test system is that they have a relatively uniform structural behaviour. Morse clusters could provide a much more varied test system, as Figure 1.7 illustrates. A suitable test would be to aim to find all the global minima at $\rho=3, 6, 10$ and 14 up to $N=80$, as putative global minima have been tabulated for this size and parameter range [15, 33]. One would generally expect the difficulty of global optimization to increase with ρ because the number of minima increases [73, 74] and the energy landscape becomes more rough [74, 75]. The system also provides many examples of structural competition, particularly for the short-ranged potentials where decahedral and close-packed clusters can have similar energies. A number of studies have begun to use Morse clusters as a test system [76, 77].

4. MULTIPLE-FUNNEL ENERGY LANDSCAPES

The aim of this section is to explain the physics that lies behind whether global optimization of a system is easy or difficult, for example, to explain the size-dependence of Figures 1.10 and 1.11. As mentioned in Section 3, an equivalent of Levinthal’s paradox, which was originally formulated to capture the difficulty of a protein folding to its native state, can be applied to a cluster locating its global minimum. The flaw in that paradox is its assumption that conformations will be sampled randomly, i.e. all configurations are equally likely, because we know that in an equilibrium physical sampling of the conformation space, say in the canonical ensemble, each point will be sampled with a probability proportional to the Boltzmann weight, $\exp(-E(\mathbf{x})/kT)$. Thus, the Boltzmann factor favours low-energy conformations. Therefore, we can begin to see the vital role played by the potential energy surface. This role extends beyond purely thermodynamic considerations to the dynamics: does the topography and connectivity of the PES naturally lead the system towards or away from the global minimum?

The Levinthal assumption of random sampling is equivalent to assuming that the energy landscape has the topography of a perfectly flat putting green with no thermodynamical or dynamical biases towards the global minimum at the bottom of the ‘hole’. Similarly, the NP-hard character of the global optimization of atomic clusters [78], which results in part from the exponential increase in the search space with size, considers a general case where no assumptions about the topography of the PES can be made. In the protein folding community, after the fallacy in the Levinthal paradox was recognized, attention focussed on the more important question of how does the topography of the PES differ for those polypeptides that are able to find their native states

from those that cannot [63]. Here, I address similar questions for the global optimization of clusters.

One of the topographical features of the energy landscape that the protein folding community has found to common is, what has been termed, a ‘funnel’ [63, 79]. By this they mean a region of configuration space that can be described in terms of a set of downhill pathways that converge on a single low-energy structure or a set of closely-related low-energy structures. As its name suggest a protein PES with a single funnel converging on the native state will be a good folder because the topography helps in guiding the protein towards that native state.

One technique that has proven to be useful in characterizing the PES topography of proteins [80, 81, 82] and clusters is the disconnectivity graph [83, 84, 85]. They provide a representation of the connectivity of the multi-dimensional energy landscape and by depicting the effective barriers between minima they are especially useful in the interpretation of dynamics.

To construct a disconnectivity graph, at a series of energy levels the minima on the PES are divided into sets which are connected by paths that never exceed that energy level. In the graph each set is represented by a node at the appropriate energy and lines connect a node to the sets at higher and lower energy which contain the minima corresponding to the original node. A line always ends at the energy of the minimum it represents.

Disconnectivity graphs can be understood by analogy to the effects of the water level in a geographical landscape. The number of nodes in a graph at a given energy is equivalent to the number of distinct seas and lakes for a given water level. Inspection of actual disconnectivity graphs, e.g. Figure 1.12, also helps to clarify these ideas. At sufficiently high energy, all minima are mutually accessible and so there is only one node, but as the energy decreases sets of minima become disconnected from each other and the graph splits, until at sufficiently low energy, again there is only one node left, that of the global minimum. The pattern of the graph can reveal particularly interesting information about the PES topography. For a PES with a single funnel there is a single dominant stem with the other minima branching directly off it as the energy is decreased. By contrast for ‘multiple-funnel’ PES’s the graph is expected to split at high energy into two or more major stems.

In Figure 1.12 disconnectivity graphs for a selection of LJ clusters are presented, in particular some of those clusters that Figures 1.10 and 1.11 indicated are more difficult to optimize. In the graph for LJ_{13} all the minima in our near-exhaustive sample are represented. The graph shows the form for an ideal single-funnel PES, because the icosahedral global minimum is particularly low in energy, and dominates the energy landscape. The PES has a remarkable connectivity: 911 distinct transition states are connected to the global minimum and all minima are within three rearrangements of the global

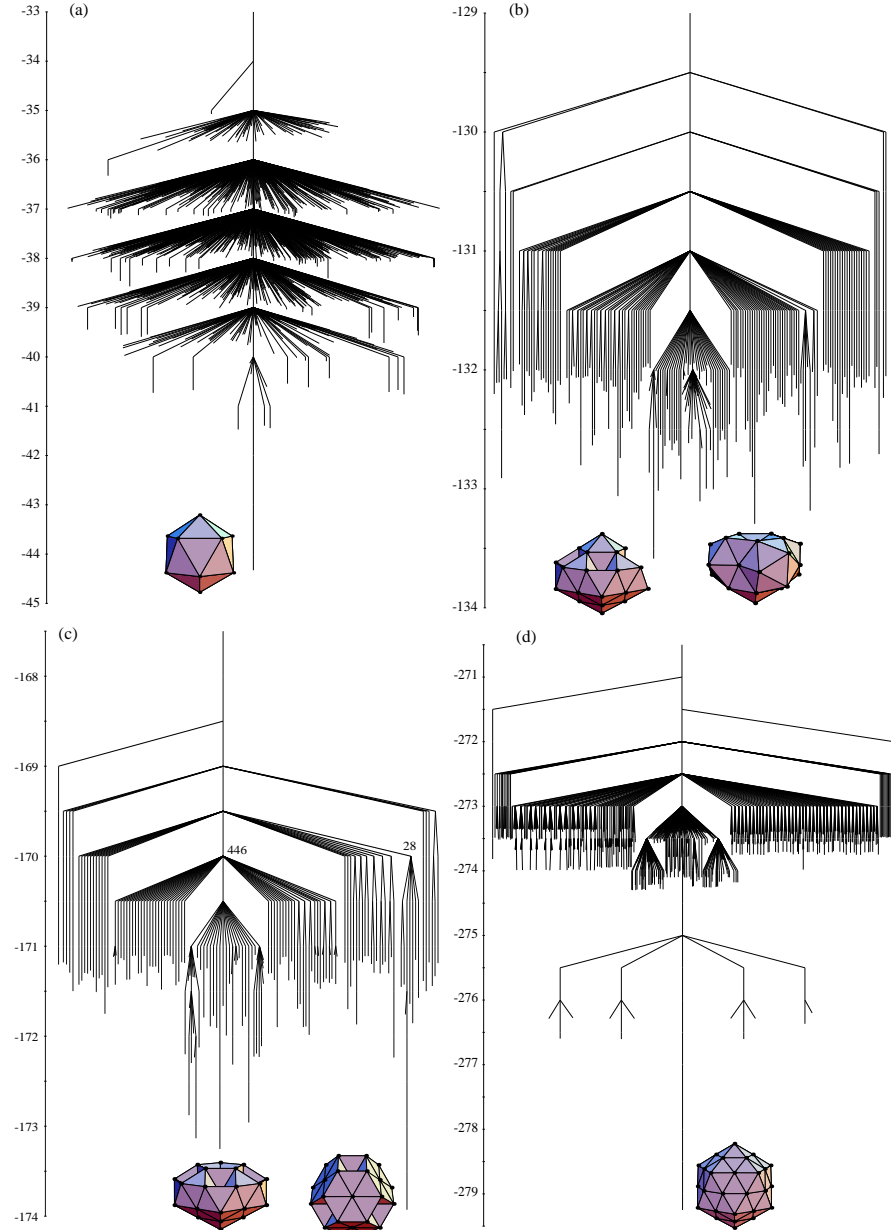


Figure 1.12 Disconnectivity graphs for (a) LJ₁₃, (b) LJ₃₁, (c) LJ₃₈, (d) LJ₅₅, (e) LJ₇₅ and (f) LJ₁₀₂. In (a) all the minima are represented. In the other parts only the branches leading to the (b) 200, (c) 150, (d) 900, (e) 250 and (f) 200 lowest-energy minima are shown. The numbers adjacent to the nodes indicate the number of minima the nodes represent. Pictures of the global minimum, and sometimes the second lowest-energy minimum, are adjacent to the corresponding branch. The units of the energy axes are ϵ .

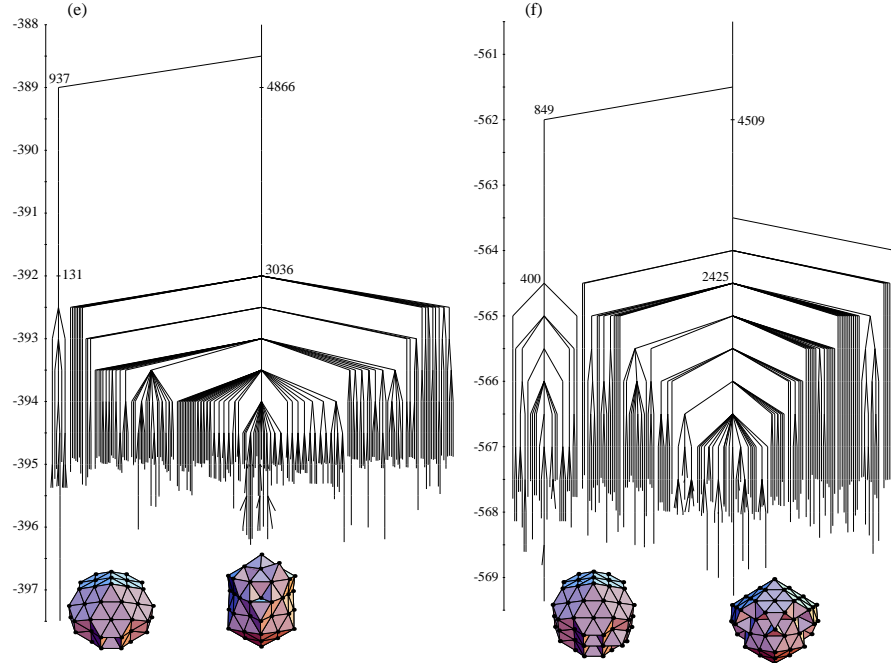


Figure 1.12 cont.

minimum. The disconnectivity graph for LJ₅₅, another ‘magic number’ LJ cluster, also has a single-funnel. Unlike, for LJ₁₃ we are unable to represent all the minima that we found on the graph, so instead we concentrate on the lower-energy minima in our sample. Indeed, the two bands of minima in the graph represent Mackay icosahedra with one or two defects. The graph only reveals the bottom of a funnel which extends up into the liquid-like minima [84].

In contrast to these two clusters, the bottom of the LJ₃₁ PES is much flatter, and there are significant barriers between the low-energy minima, in particular between the two lowest-energy minima, which are icosahedral structures, but with different types of surface overlayer. These effects of structural competition are found in more extreme form in the graphs of those clusters with non-icosahedral global minima. The graphs of LJ₃₈, LJ₇₅ and LJ₁₀₂ split at high energy into stems associated with icosahedral and fcc or decahedral structures, and so these energy landscapes have two major funnels. This splitting is most dramatic for LJ₇₅ and LJ₁₀₂, where the barrier between the two funnels is much greater than between any of the other sets of minima. The barriers between the two lowest-energy minima are 4.22ϵ and 3.54ϵ for LJ₃₈, 8.69ϵ and 7.48ϵ for LJ₇₅ and 7.44ϵ and 7.36ϵ for LJ₁₀₂. The corresponding lowest-barrier paths are represented in Figure 1.13. These pathways pass over many transition states—

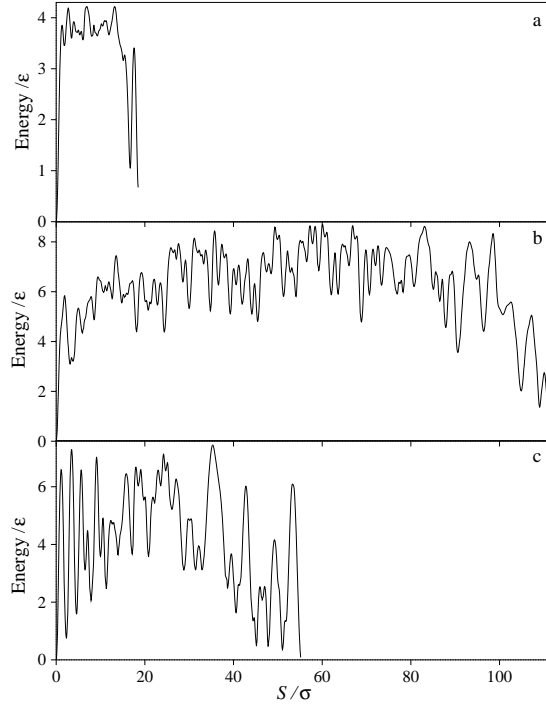


Figure 1.13 The lowest-energy path from the global minimum to the second lowest-energy minimum for (a) LJ_{38} , (b) LJ_{75} and (c) LJ_{102} . In each case the zero of energy corresponds to the energy of the global minimum.

13, 65 and 30 for LJ_{38} , LJ_{75} and LJ_{102} , respectively. There are many other pathways connecting the funnels, but they are either longer or involve higher effective barriers. For LJ_{38} the pathway passes through disordered liquid-like minima. However, for the two larger clusters all the minima along the pathways are ordered and the main structural changes are achieved by rearrangements that involve cooperative twists around the five-fold axis of the decahedron—the conservation of this axis throughout the structural transformation has also been observed in simulations of the decahedral to icosahedral transition in gold clusters [14]. For LJ_{75} the Marks decahedron is oblate whilst the low-energy icosahedral minima are prolate, so the pathway involves a greater amount of reorganization of the surface layer either side of these cooperative transitions than for LJ_{102} , for which the decahedral and icosahedral structures have fairly similar shapes. Hence the shorter pathway for LJ_{102} (Figure 1.13), even though it is larger.

As expected from the general dominance of icosahedral structures in this size range, there are many more low-energy icosahedral minima than low-energy decahedral or fcc minima for these three clusters. There are many

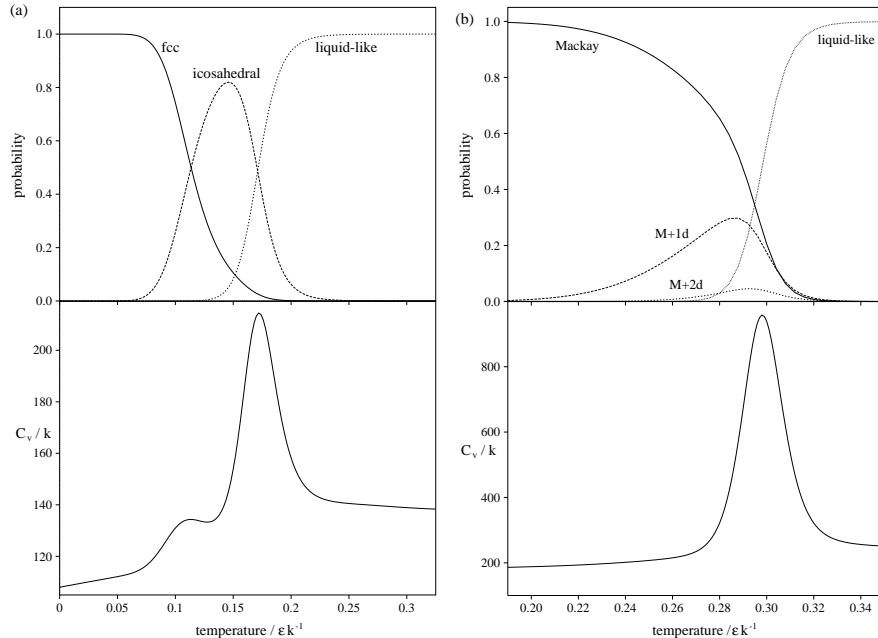


Figure 1.14 Equilibrium thermodynamic properties of (a) LJ₃₈ and (b) LJ₅₅ in the canonical ensemble. Both the probability of the cluster being in the labelled regions of configuration space and the heat capacity, C_v are depicted. The label M+nd stands for a Mackay icosahedron with n surface defects.

low-energy arrangements of the incomplete surface layer of the icosahedral structures, whereas the decahedral or fcc structures have especially compact structures and so any alteration in structure leads to a significant increase in energy. The number of minima in our samples that lie within the respective funnels is marked on Figure 1.12 and is indicative of the greater width of the icosahedral funnels.

From characterizing the energy landscapes of these clusters, the physical origins of some of the differences in difficulty for GO algorithms should be becoming apparent. The single funnels of LJ₁₃ and LJ₅₅ make the global minimum particularly accessible, and the system is strongly directed towards the global minimum on relaxation down the PES. For LJ₃₁, once the system has reached a low-energy structure, the flatness and the barriers at the bottom of the PES mean that further optimization is relatively slow compared to LJ₁₃ and LJ₅₅. For the clusters with non-icosahedral global minima, the icosahedral funnel is much more accessible because of its greater width. Furthermore, after entering the icosahedral funnel, subsequent escape into the fcc or decahedral funnel is likely to be very slow because of the large barriers that need to be overcome. The icosahedral funnel acts as a kinetic trap hindering global optimization. These effects will come out even more clearly in the next two

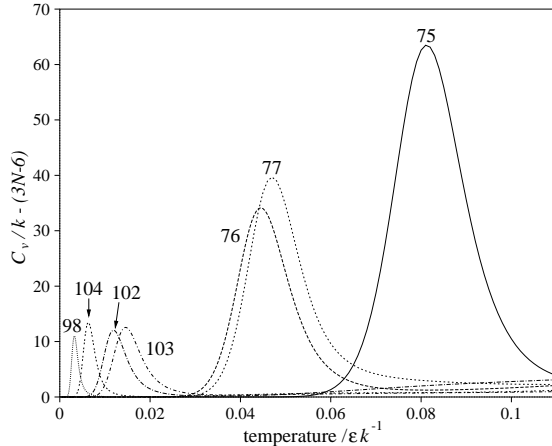


Figure 1.15 Canonical heat capacity peaks associated with the structural transitions from the global minimum to icosahedral structures for the LJ clusters with non-icosahedral global minima. The sizes are as labelled.

sections as we look at the thermodynamics and dynamics associated with these clusters. From the disconnectivity graphs one would expect trapping to be a significantly greater hindrance to global optimization for LJ_{75} and LJ_{102} than for LJ_{38} , and the longer interfunnel pathway for LJ_{75} provides a possible explanation of why LJ_{102} seems to be somewhat less difficult to optimize than LJ_{75} .

4.1 THERMODYNAMICS

The typical thermodynamic properties of a cluster are illustrated in Figure 1.14b for LJ_{55} . The heat capacity peak is associated with a melting transition that is the finite-size analogue of a first-order phase transition [86] and up to melting the structure is based on the global minimum, perhaps with some surface defects. The thermodynamics of the clusters with non-icosahedral structures are significantly different. Now, as well as the melting transition there is a further transition associated with a transition from the global minimum to the icosahedral structures that gives rise to a second lower-temperature peak in the heat capacity (Figure 1.14a and 1.15). For LJ_{38} the transition occurs fairly close to melting,⁴ however as the size increases the transition temperature generally decreases [43].

These solid-solid transitions have a number of implications for global optimization. Firstly, on cooling from the melt it is thermodynamically more favourable for the cluster to enter the icosahedral funnel than that associated with the global minimum. Secondly, the transitions, particularly those for the larger clusters, lie below the ‘glass transition’ temperature where the cluster is effectively trapped in the current local minimum. This presents a nightmare

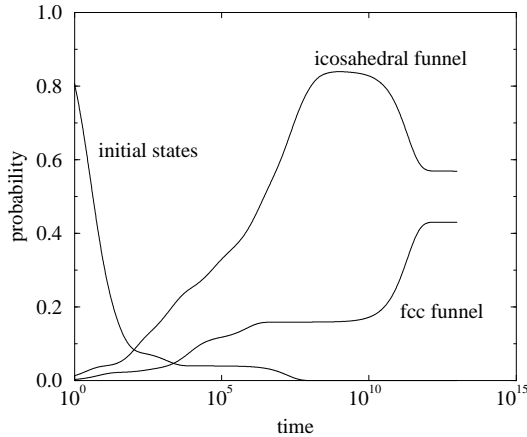


Figure 1.16 Relaxation of LJ₃₈ from high-energy minima showing the fast and slow contributions to the final probability of the fcc funnel. The time is in units of $(mo^2/\epsilon)^{1/2}$.

scenario for simulated annealing. On cooling the cluster would first enter the icosahedral funnel, where it would then become trapped, even when the global minimum becomes thermodynamically more stable, because of the large free energy barriers (relative to kT) for escape from this funnel [87].

In the protein folding literature, good folders have been shown to have a large value of the ratio of folding temperature to the glass transition temperature, T_f/T_g , because this ensures the kinetic accessibility of the native state of the protein at temperatures where it is thermodynamically most favoured [63]. By contrast, these clusters have effective T_f/T_g values less than one and are archetypal ‘bad folders’.

4.2 DYNAMICS

From the large samples of minima and transition states used to construct the disconnectivity graphs it is possible to calculate the rate of interfunnel passage using a master equation approach [75, 85]. The rate constants for LJ₃₈ have been computed and show that the interfunnel dynamics obeys an Arrhenius law well with the activation energies corresponding to the barriers associated with the lowest-energy pathway between the two funnels [75, 85]. For LJ₃₈ this gives a value of 43 s⁻¹ for the interfunnel rate constant at the centre of the fcc to icosahedral transition (using parameters appropriate for Ar). This is beyond the time scales accessible to molecular dynamics simulations. The equivalent rate constants for the larger clusters are much slower because of the larger activation energies and the lower transition temperatures.

Figure 1.16 illustrates for LJ₃₈ the dynamics of relaxation from high-energy states. The initial relaxation is relatively rapid and the majority of the population enters the icosahedral funnel (the approximations in this calculation

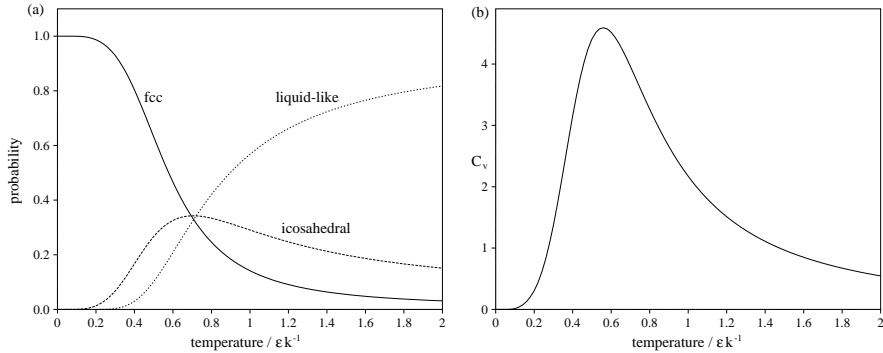


Figure 1.17 Equilibrium thermodynamic properties of LJ₃₈ on the transformed PES in the canonical ensemble. (a) The probability of the cluster being in the fcc, icosahedral and liquid-like regions of configuration space. (b) The configurational heat capacity, C_v .

actually lead to an overestimation of the probability of initially entering the fcc funnel). These processes are separated by a couple of decades in time from the subsequent equilibration between the two funnels.

The combined effects of the thermodynamics and dynamics can be illustrated by some simulated annealing results. For LJ₅₅ the probability of reaching the global minimum in annealing simulations of 10^6 and 10^7 MC cycles is 29% and 94%. The equivalent values for LJ₃₈ are 0% and 2% and for LJ₇₅ the annealing simulations were never able to locate the global minimum.

4.3 OPTIMIZATION SOLUTIONS

The previous sections illustrate the difficulty of finding the global minimum of the LJ clusters with non-icosahedral global minima if the natural thermodynamics and dynamics of the system are followed. However, optimization approaches do not have to be restricted to this behaviour. For example, as we mentioned in Section 3 the basin-hopping transformation accelerates the dynamics, allowing hops directly between basins. However, the transformation only reduces the interfunnel energy barriers by 0.68ϵ for LJ₃₈, 0.86ϵ for LJ₇₅ and 0.89ϵ for LJ₇₅. Therefore, multiple-funnels are still potentially problematic.

Figure 1.17 shows that the thermodynamic properties of LJ₃₈ are dramatically changed by the transformation. The transitions have been significantly broadened. There is now only a single heat capacity peak and a broad temperature range where all states are populated. In particular, the global minimum now has a significant probability of occupation at temperatures where the free energy barriers between the funnels can be surmounted. This effect can be seen in the basin-hopping simulations: the cluster is still much more likely to enter the icosahedral funnel during the initial rapid relaxation down the PES,

but the cluster can now also pass back and forth between the two funnels at a reasonable rate [52].

This broadened thermodynamics also reduces the difficulty of global optimization for the larger non-icosahedral clusters, making it possible, if still very difficult, to reach the global minimum. However, the results of Leary indicate that for these clusters it is more efficient to restart a run when it gets stuck in a funnel (and hope that it enters the funnel of the global minimum next time) than to wait for the cluster to escape from that funnel [65].

We can understand why the PES transformation so dramatically changes the thermodynamics of the system, by examining p_i , the occupation probability of a minimum i . For the untransformed PES within the harmonic approximation $p_i \propto \exp(-\beta E_i)/\bar{\nu}_i^{3N-6}$, where E_i is the potential energy of minimum i and $\bar{\nu}_i$ is the geometric mean vibrational frequency. For the transformed PES $p_i \propto A_i \exp(-\beta E_i)$, where A_i is the hyperarea of the basin of attraction of minimum i . The differences between these expressions, the vibrational frequency and hyperarea terms, have opposite effects on the thermodynamics. The higher-energy minima are generally less rigid and so the vibrational term entropically stabilizes the icosahedra and, even more so, the liquid-like state, pushing the transitions down to lower temperature and sharpening them. By contrast the hyperarea of the minima decreases with increasing potential energy, thus stabilizing the lower-energy states and broadening the thermodynamics.

5. CONCLUSIONS

In this chapter I hope to have shown how physical insight can play an important role in understanding the behaviour of global optimization algorithms and hope that these insights can help provide a firmer physical (rather than just empirical or intuitive) foundation for the design of new improved algorithms.

In particular I have highlighted some examples where a multiple-funnel energy landscape strongly hinders global optimization. Such challenging cases are likely to be a common feature for any cluster system where there is not a single strongly dominant structural type. More generally, multiple funnels probably represent the most difficult problem for this class of GO problems, in which the lowest-energy configuration of a system is sought. For example, for this reason, the main criterion in the design of polypeptides that fold well is the avoidance of multiple funnels by optimizing the energy gap between the native state and competing low-energy structures [88].

I have also shown why the basin-hopping transformation of the energy landscape makes global optimization for these multiple-funnel cases easier. The method's success results from a broadening of the thermodynamics, so that the occupation probability of the global minimum is significant at temperatures where the interfunnel free energy barriers can be surmounted. This idea should

act as a design principle in the development of any new GO algorithms that hope to overcome the challenge of multiple funnels.

Although basin-hopping is successful for the LJ multiple-funnel examples, further improvements in efficiency are required before one can hope to succeed for similar cases at larger size or for potential energy functions that are significantly more computationally intensive to evaluate. A number of avenues by which this may be achieved suggest themselves. Firstly, the basin-hopping algorithm searches the transformed potential energy surface using simple MC. However, there are a whole raft of methods that have been developed in order to speed up the rate of rare events in simulations on the untransformed PES, which could potentially be applied to the transformed PES. These include parallel tempering [89], jump-walking [90], and the use of non-Boltzmann ensembles, such as Tsallis statistics [6].

Secondly, the basin-hopping transformation can be combined with other PES transformations, of which there have been many suggestions [91], to get a double transformation (and hopefully a greater simplification) of the PES [92]. The potential problem with this type of approach is that as well as smoothing the PES, most transformations also change the relative stabilities of different structures. This can work in one's favour if the transformation stabilizes the global minimum. For example, a recent transformation proposed by Locatelli and Schoen, which favours compact spherical clusters, stabilizes the non-icosahedral LJ global minima [71]; for the 38-atom cluster the PES, when sufficiently deformed, has a single-funnel topography with the truncated octahedron at its bottom [92]. But just as often a transformation will destabilize the global minimum—this is why the performance of many PES-transformation GO methods is erratic, perhaps solving some ‘hard’ instances while failing for ‘easier’ examples. However, the proposed approach could be run alongside standard basin-hopping runs, and so would perhaps succeed in instances where the standard algorithm struggles.

Thirdly, Hartke recently proposed a modification to the genetic algorithm approach, in which a diversity of structures is maintained in the population [47]. This leads to significant increases in efficiency for the LJ clusters with multiple-funnels, because it prevents the whole population being confined (and trapped) within the icosahedral funnel. Such an approach could also potentially increase the efficiency of other algorithms. For example, a diversity of structures could be maintained between a set of parallel basin-hopping runs.

Acknowledgments

The author is the Sir Alan Wilson Research Fellow at Emmanuel College, Cambridge. I would like to acknowledge the role played by David Wales and Mark Miller in this research program and to thank Bob Leary for providing the data for Figure 1.11.

Notes

1. One of the values reported in Table 1 of Ref. [33] has been superseded. At $N=30$ and $\rho=14$ the energy of the global minimum is -106.835 790.
2. In this sense I should refer to the lowest known structures only as *putative* global minima, but for convenience I usually drop this adjective.
3. A copy of this difficult to locate citation classic (Ref. [60]) can be found on the web at <http://brian.ch.cam.ac.uk/~mark/levinthal/levinthal.html>.
4. The thermodynamic properties illustrated in Figures 1.14 and 1.15 have been calculated using a method where the thermodynamic properties of the individual minima are summed [85, 93]. However, recent simulations using parallel tempering indicate that for LJ₃₈ the two transitions are slightly closer than indicated by Figure 1.14 and so the fcc to icosahedral transition results only in a shoulder in the heat capacity curve [72].

References

- [1] D. Frenkel and B. Smit, *Understanding Molecular Simulation* (Academic Press, San Diego, 1996).
- [2] S. Kirkpatrick, C. D. Gelatt, and M. P. Vecchi, *Science* **220**, 671 (1983).
- [3] C. Tsallis, *J. Stat. Phys.* **52**, 479 (1998).
- [4] C. Tsallis, *Braz. J. Phys.* **29**, 1 (1999).
- [5] C. Tsallis and D. A. Stariolo, *Physica A* **233**, 395 (1996).
- [6] I. Andricoaei and J. E. Straub, *Phys. Rev. E* **53**, R3055 (1996).
- [7] D. E. Goldberg, *Genetic Algorithms in Search, Optimization, and Machine Learning* (Addison-Wesley, Reading, 1989).
- [8] B. Hartke, in *Case Studies in Global Optimization*, edited by J. Pinter (Kluwer Academic, Dordrecht, 2000).
- [9] D. J. Wales and J. P. K. Doye, *J. Phys. Chem. A* **101**, 5111 (1997).
- [10] I. A. Harris, R. S. Kidwell, and J. A. Northby, *Phys. Rev. Lett.* **53**, 2390 (1984).
- [11] T. P. Martin, *Phys. Rep.* **273**, 199 (1996).
- [12] E. K. Parks, G. C. Niemann, K. P. Kerns, and S. J. Riley, *J. Chem. Phys.* **107**, 1861 (1997).
- [13] M. M. Alvarez *et al.*, *Chem. Phys. Lett.* **266**, 91 (1997).
- [14] C. L. Cleveland, W. D. Luedtke, and U. Landman, *Phys. Rev. Lett.* **81**, 2036 (1998).
- [15] J. P. K. Doye, D. J. Wales, and R. S. Berry, *J. Chem. Phys.* **103**, 4234 (1995).
- [16] L. D. Marks, *Phil. Mag. A* **49**, 81 (1984).
- [17] A. L. Mackay, *Acta Cryst.* **15**, 916 (1962).
- [18] J. P. K. Doye and D. J. Wales, *Chem. Phys. Lett.* **247**, 339 (1995).

- [19] B. Raoult, J. Farges, M. F. de Feraudy, and G. Torchet, *Phil. Mag. B* **60**, 881 (1989).
- [20] R. H. Leary and J. P. K. Doye, *Phys. Rev. E* **60**, R6320 (1999).
- [21] W. Branz, N. Malinowski, H. Schaber, and T. P. Martin, *Chem. Phys. Lett.* accepted (2000).
- [22] J. E. Jones and A. E. Ingham, *Proc. R. Soc. A* **107**, 636 (1925).
- [23] L. T. Wille, in *Annual Reviews of Computational Physics VII*, edited by D. Stauffer (World Scientific, Singapore, 2000).
- [24] J. A. Northby, *J. Chem. Phys.* **87**, 6166 (1987).
- [25] S. Gomez and D. Romero, *Proceedings of the First European Congress of Mathematics* (Birkhauser, Basel, 1994), Vol. III, pp. 503–509.
- [26] J. Pillardy and L. Piela, *J. Phys. Chem.* **99**, 11805 (1995).
- [27] D. Romero, C. Barrón, and S. Gómez, *Comp. Phys. Comm.* **123**, 87 (1999).
- [28] P. M. Morse, *Phys. Rev.* **34**, 57 (1929).
- [29] D. J. Wales, L. J. Munro, and J. P. K. Doye, *J. Chem. Soc., Dalton Trans.* 611 (1996).
- [30] L. A. Girifalco, *J. Phys. Chem.* **96**, 858 (1992).
- [31] D. J. Wales and J. Uppenbrink, *Phys. Rev. B* **50**, 12342 (1994).
- [32] L. A. Girifalco and V. G. Weizer, *Phys. Rev.* **114**, 687 (1959).
- [33] J. P. K. Doye and D. J. Wales, *J. Chem. Soc., Faraday Trans.* **93**, 4233 (1997).
- [34] T. P. Martin, T. Bergmann, H. Göhlich, and T. Lange, *Chem. Phys. Lett.* **172**, 209 (1990).
- [35] D. R. Nelson and F. Spaepen, *Solid State Phys.* **42**, 1 (1989).
- [36] F. C. Frank and J. S. Kasper, *Acta Cryst.* **11**, 184 (1958).
- [37] F. C. Frank and J. S. Kasper, *Acta Cryst.* **12**, 483 (1959).
- [38] F. Dassenoy *et al.*, *J. Chem. Phys.* **112**, 8137 (2000).
- [39] M. Dzugutov and U. Dahlborg, *J. Non-Cryst. Solids* **131-133**, 62 (1991).
- [40] M. Dzugutov, *Phys. Rev. A* **46**, R2984 (1992).
- [41] M. Dzugutov, *Phys. Rev. Lett.* **70**, 2924 (1993).
- [42] J. P. K. Doye and D. J. Wales, *Phys. Rev. Lett.* **80**, 1357 (1998).
- [43] J. P. K. Doye and F. Calvo, *Phys. Rev. Lett.* to be submitted .
- [44] F. Baletto, C. Mottet, and R. Ferrando, *Phys. Rev. Lett.* **84**, 5544 (2000).
- [45] C. D. Maranas and C. A. Floudas, *J. Chem. Phys.* **97**, 7667 (1992).

- [46] D. M. Deaven, N. Tit, J. R. Morris, and K. M. Ho, *Chem. Phys. Lett.* **256**, 195 (1996).
- [47] B. Hartke, *J. Comp. Chem.* **20**, 1752 (1999).
- [48] M. D. Wolf and U. Landman, *J. Phys. Chem. A* **102**, 6129 (1998).
- [49] Z. Li and H. A. Scheraga, *Proc. Natl. Acad. Sci. USA* **84**, 6611 (1987).
- [50] G. L. Xue, *J. Glob. Opt.* **4**, 187 (1994).
- [51] D. M. Deaven and K. M. Ho, *Phys. Rev. Lett.* **75**, 288 (1995).
- [52] J. P. K. Doye, D. J. Wales, and M. A. Miller, *J. Chem. Phys.* **109**, 8143 (1998).
- [53] D. Liu and J. Nocedal, *Mathematical Programming B* **45**, 503 (1989).
- [54] R. P. White and H. R. Mayne, *Chem. Phys. Lett.* **289**, 463 (1998).
- [55] P. Derreumaux, *Theor. Chem. Acc.* **104**, 1 (2000).
- [56] I. Rata *et al.*, *Phys. Rev. Lett.* **85**, 546 (2000).
- [57] D. J. Wales and H. A. Scheraga, *Science* **285**, 1368 (1999).
- [58] F. H. Stillinger, *Phys. Rev. E* **59**, 48 (1999).
- [59] C. J. Tsai and K. D. Jordan, *J. Phys. Chem.* **97**, 11227 (1993).
- [60] C. Levinthal, in *Mössbauer Spectroscopy in Biological Systems, Proceedings of a Meeting Held at Allerton House, Monticello, Illinois*, edited by J. T. P. DeBrunner and E. Munck (University of Illinois Press, Illinois, 1969), pp. 22–24.
- [61] R. Zwanzig, A. Szabo, and B. Bagchi, *Proc. Natl. Acad. Sci. USA* **89**, 20 (1992).
- [62] R. Zwanzig, *Proc. Natl. Acad. Sci. USA* **92**, 9801 (1995).
- [63] J. D. Bryngelson, J. N. Onuchic, N. D. Socci, and P. G. Wolynes, *Proteins: Structure, Function and Genetics* **21**, 167 (1995).
- [64] J. P. K. Doye and D. J. Wales, *J. Chem. Phys.* **105**, 8428 (1996).
- [65] R. H. Leary, *J. Glob. Opt.* in press (2000).
- [66] J. A. Niesse and H. R. Mayne, *J. Chem. Phys.* **105**, 4700 (1996).
- [67] K. Michaelian, *Chem. Phys. Lett.* **293**, 202 (1998).
- [68] R. V. Pappu, R. K. Hart, and J. W. Ponder, *J. Phys. Chem. B* **102**, 9725 (1998).
- [69] J. Pillardy, A. Liwo, and H. A. Scheraga, *J. Phys. Chem. A* **103**, 9370 (1999).
- [70] D. B. Faken, A. F. Voter, D. L. Freeman, and J. D. Doll, *J. Phys. Chem. A* **103**, 9521 (1999).
- [71] M. Locatelli and F. Schoen, *Computational Optimization and Applications* submitted (2000).

- [72] J. P. Neirotti, F. Calvo, D. L. Freeman, and J. D. Doll, *J. Chem. Phys.* **112**, 10340 (2000).
- [73] J. P. K. Doye and D. J. Wales, *J. Phys. B* **29**, 4859 (1996).
- [74] M. A. Miller, J. P. K. Doye, and D. J. Wales, *J. Chem. Phys.* **110**, 328 (1999).
- [75] M. A. Miller, J. P. K. Doye, and D. J. Wales, *Phys. Rev. E* **60**, 3701 (1999).
- [76] C. Roberts, R. L. Johnston, and N. T. Wilson, *Theor. Chem. Acc.* **104**, 123 (2000).
- [77] H. Xu and B. J. Berne, *J. Chem. Phys.* **112**, 2701 (2000).
- [78] L. T. Wille and J. Vennik, *J. Phys. A* **18**, L419 (1985).
- [79] P. E. Leopold, M. Montal, and J. N. Onuchic, *Proc. Natl. Acad. Sci. USA* **89**, 8271 (1992).
- [80] O. M. Becker and M. Karplus, *J. Chem. Phys.* **106**, 1495 (1997).
- [81] Y. Levy and O. M. Becker, *Phys. Rev. Lett.* **81**, 1126 (1998).
- [82] M. A. Miller and D. J. Wales, *J. Chem. Phys.* **111**, 6610 (1999).
- [83] D. J. Wales, M. A. Miller, and T. R. Walsh, *Nature* **394**, 758 (1998).
- [84] J. P. K. Doye, M. A. Miller, and D. J. Wales, *J. Chem. Phys.* **111**, 8417 (1999).
- [85] D. J. Wales *et al.*, *Adv. Chem. Phys.* in press (2000).
- [86] P. Labastie and R. L. Whetten, *Phys. Rev. Lett.* **65**, 1567 (1990).
- [87] J. P. K. Doye, M. A. Miller, and D. J. Wales, *J. Chem. Phys.* **110**, 6896 (1999).
- [88] R. Goldstein, Z. Luthey-Schulten, and P. G. Wolynes, *Proc. Natl. Acad. Sci. USA* **89**, 4918 (1992).
- [89] E. Marinari and G. Parisi, *Europhys. Lett.* **19**, 451 (1992).
- [90] D. D. Frantz, D. L. Freeman, and J. D. Doll, *J. Chem. Phys.* **93**, 2769 (1990).
- [91] S. Schelstrate, W. Schepens, and H. Verschelde, in *Molecular Dynamics: From Classical to Quantum Mechanics*, edited by P. B. Balbuena and J. M. Seminario (Elsevier, Amsterdam, 1999), pp. 129–185.
- [92] J. P. K. Doye, *Phys. Rev. E* submitted (cond-mat/0001066).
- [93] J. P. K. Doye and D. J. Wales, *J. Chem. Phys.* **102**, 9659 (1995).